J Fluoresc (2011) 21:663–672
DOI 10.1007/s10895-010-0754-6

ORIGINAL PAPER

Towards Nanoscale Biomedical Devices in Medicine: Biofunctional and Spectroscopic Characterization of Superparamagnetic Nanoparticles

Antonietta Parracino · Gnana Prakash Gajula · Ane Kold di Gennaro · Maria Teresa Neves-Petersen · Jens Rafaelsen · Steffen B. Petersen

Received: 28 June 2010 / Accepted: 18 October 2010 / Published online: 25 November 2010

Abstract Medical interest in nanotechnology originates from a belief that nanoscale therapeutic devices can be constructed and directed towards its target inside the human body. Such nanodevices can be engineered by coupling superparamagnetic nanoparticle to biomedically active proteins. We hereby report the immobilization of a PhEst, a S-formylglutathione hydrolase from the psychrophilic *P. haloplanktis* TAC125 onto the gold coated surface of modified superparamagnetic core-shell nanoparticles (Fe_3O_4@Au). The synthesis of the nanoparticles is also reported. S-formylglutathione hydrolases constitute a family of ubiquitous enzymes which play a key role in formaldehyde detoxification both in prokaryotes and eukaryotes. PhEst was originally annotated as a putative feruloyl esterase, an enzyme that releases ferulic acid (an antioxidant reactive towards free radicals such as reactive oxygen species) from polysaccharides esters. Dynamic light scattering, scanning electron microscopy with energy dispersive X-ray spectroscopy, UV–visible absorption spectroscopy, fluorescence spectroscopy, magnetic separation technique and enzyme catalytic assay confirmed the chemical composition of the gold covered superparamagnetic nanoparticles, the binding and activity of the enzyme onto the nanoparticles. Activity data in U/ml confirmed that the immobilized enzyme is approximately 2 times more active than the free enzyme in solution. Such particles can be directed with external magnetic fields for bio-separation and focused towards a medical target for therapeutical as well as bio-sensor applications.

Keywords Superparamagnetic gold nanoparticles · Core-shell nanoparticles · Bioseparation · Esterase · Bioconjugation

Abbreviations

BSA	Bovine serum albumin
DLS	Dynamic light scattering
DPPH	1,1-diphenyl-2picrylhydrazyl
EDS	Energy dispersive X-ray spectroscopy
Fe_3O_4@Au	Superparamagnetic core(magnetite)-shell (gold) nanoparticles
MRI	Magnetic resonance imaging
PhEst	Putative feruloyl esterase
pNPAc	p-nitro phenyl acetate
ROS	Reactive oxygen species
SEM	Scanning electron microscopy
U/ml	Unit/milliliter (1 unit U is the amount of enzyme that catalyses the reaction of 1 μmol of substrate per minute)
UV–visible	Ultraviolet–visible
FWHM	Full width at half maximum

Antonietta Parracino and Gnana Prakash Gajula contributed equally to the paper.

A. Parracino · G. P. Gajula · A. K. di Gennaro · M. T. Neves-Petersen · S. B. Petersen (✉)
NanoBiotechnology Group,
Department of Physics and Nanotechnology, Aalborg University,
Skjernvej 4A,
Aalborg, Denmark
e-mail: sp@nano.aau.dk

J. Rafaelsen
Department of Physics and Nanotechnology, Aalborg University,
Skjernvej 4A,
Aalborg, Denmark

S. B. Petersen
The Institute for Lasers, Photonics and Biophotonics,
University at Buffalo, The State University of New York Buffalo,
Buffalo, NY 14260-3000, USA

Introduction

For the last few decades, research efforts have been focused on the development of new materials at the nanoscale in order to explore structures, devices and systems with novel properties. The physico-chemical properties of materials at nanoscale can be precisely tuned by modifying their size, shape and composition [1, 2]. Among various nano materials, magnetic core-shell particles have been commonly used in many technological applications, especially for biological applications such as drug targeting and delivery, cell labeling and separation, cancer therapy, magnetic resonance imaging (MRI) contrast agents, biosensors and bioimaging [3, 4]. Core-shell particles that result from the combination of different metals display novel properties compared to their monometallic counterparts. Among core-shell nanoparticles, Fe_3O_4@Au particles are widely used due to chemical stability, good biocompatibility, low toxicity, easy dispersibility, affinity towards biomolecules with amine/thiol/carboxylic terminal groups and convenient preparation techniques. Super-paramagnetic iron oxides nanoparticles are being used extensively for biosciences in various applications [5]. New properties such as tunable colors by varying the thickness of gold shell and metal interaction with flourophores can be applied in fluorescent bioimaging applications and in the development of various clinical diagnosis methods [6]. Plasmonic surfaces such as gold are also known to induce quenching of excited states via energy transfer to the gold surface, which is a phenomenon of considerable interest in biophotonics [7].

Since biomolecules are highly sensitive to pH, temperature and chemical environment, immobilization protocols should maintain molecular activity and stability. Recent studies demonstrated that the incorporation of chiral molecules onto nanoparticles may facilitate nucleic recognition e.g. achieving specificity towards a protein surface [8]. Immobilization of trypsin onto super-paramagnetic nanoparticles permits higher enzyme concentrations than using free enzyme molecules, leading to shorter digestion time, and allowing also for easy separation from bulk solution [9]. Immobilization of enzymes also increases pH-stability, temperature stability, stability towards chemical denaturants and organic solvents [10]. Water soluble carbodiimide was used to activate the direct adsorption of glucose oxidase, streptokinase, chymotrypsin, dispase, BSA and alkaline phosphatase onto magnetic particles [11, 12]. Recently, decanthiol capped gold nanoparticles were modified with dithiobis (succinimidyl propionate) for bovine serum albumin (BSA) coupling by ligand exchange [3]. Brewer et al. have proposed an electrostatic interaction between BSA and citrate stabilized gold surface [13]. Among the possible interactions between amino acidic residues and gold surfaces, the interaction between thiol groups of cysteine residues and the gold surface is preferred [14, 15].

Esterases are good model systems for studies of protein structure/function relationship. Furthermore, they are widely used in technological applications such as in agro-food, detergent and pharmaceutical industries. Esterases act as biocatalysts, hydrolyzing acylglycerides and other fatty-acid esters and are also used in the synthesis of optically active compounds. These enzymes have broad substrate specificity, allowing them to access different carbon sources and to be involved in catabolic pathways. The enzyme used in our studies, PhEst, is a S-formylglutathione hydrolases(PhEst) [16–18]. S-formylglutathione hydrolases (FGHs) constitute a family of ubiquitous enzymes which play a key role in formaldehyde detoxification both in prokaryotes and eukaryotes, catalyzing the hydrolysis of S-formylglutathione to formic acid and glutathione [18]. PhEst was originally annotated as a feruloyl esterase which can be used for the isolation of ferulic acid with medical value that is present in many plants as polysaccharides esters [16–18]. Ferulic acid, like many phenols, is an antioxidant reactive towards free radicals which are implicated in DNA damage, cancer, and accelerated cell aging; the activity of ferulic compouds is widely studied using 1,1-diphenyl-2picrylhydrazyl (DPPH) as radical scavenging assay [19]. PhEst structure has recently been solved [18] and shows the typical features of the α/β-hydrolase fold: it consists of a central nine-stranded mixed β-sheet surrounded by nine α-helices, four 3_{10}-helices, and one π-helix (Fig. 1). S-formylglutathione hydrolases shows remarkable sequence conservation: cysteine residues are conserved, as well as the sequence motif (GHSMGG) containing the catalytic serine, which together with an aspartate and a histidine residue completed the hydrolase catalytic triad [18].

We here report the synthesis of Fe_3O_4@Au core-shell nanoparticles and the immobilization of the putative ferulic esterase enzyme onto the magnetic core-shell nanoparticles surface, and its enzymatic activity. We will discuss likely binding mechanism between the esterase and the gold coated nanoparticles. The magnetic properties of the enzyme decorated onto core shell nanoparticles imply that enzymatic activity can be guided towards a special target with external magnetic field. We envisage that this approach is possible in principle for any protein. We will commence studies on peptide hormones and cancer pharmaceuticals that can be directed towards a particular target inside the body.

Materials and Methods

Materials

For the synthesis of Fe_3O_4@Au core-shell nanoparticles, $FeSO_4.7H_2O$, $FeCl_3$, 25% aqueous NH_3, Sodium Citrate, $HAuCl_4$, ethanol were purchased from E-Merck. All

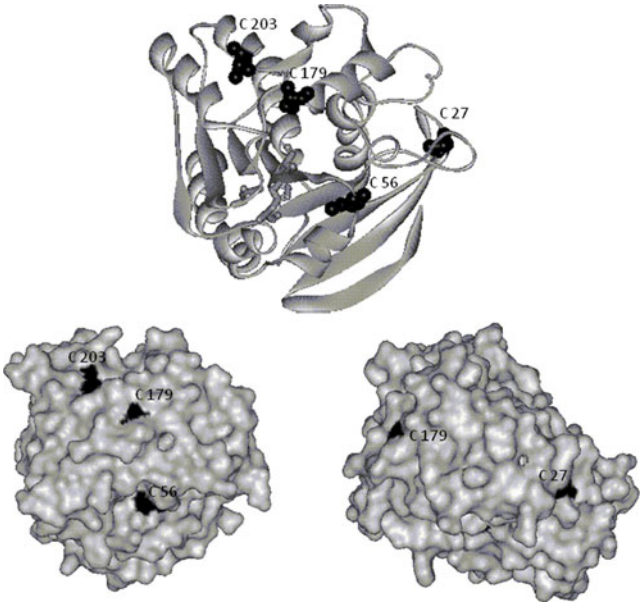

Fig. 1 3D representation of PhEst hydrolase (PDB code: 3ls2). The *upper structure* represents the monomer of the enzyme; cysteine residues are highlighted in *black* CPK. Cys10, Cy60, Cys219 are solvent accessible. The catalytic triad is composed by Ser147, Asp225 and His258 highlighted in *grey stick*. The *lower structures* show the solvent accessible surface of the monomer (*left structure* has the same orientation as the monomer displayed on *top*, and the *right structure* has been rotated 90°). All four cysteine residues are shown to be solvent accessible

chemicals were GR-grade and used without any further purification. Putative feruloyl esterase from *P. haloplanktis* TAC125 was kindly obtained from Dr. Sabato D'Auria lab, Institute of protein biochemistry, CNR, Naples, Italy. The gene coding for this esterase was cloned and expressed in *Escherichia coli cells*. The molecular weight of the monomeric form of this enzyme is 30,887 Da. The native form of the esterase is a dimer having a molecular weight of about 60 KDa. Optimum activities have been reported at pH 8.0 and optimal temperature for enzyme activity is 20 °C [17].

Preparation of Fe_3O_4@Au Core-Shell Nanoparticles

Synthesis of magnetite nanoparticles was carried out by precipitating freshly prepared iron salts in alkaline medium [20]. Acidic solutions of 0.1 M $FeSO_4.7H_2O$ and 0.2 M $FeCl_3$ were mixed in 1:1 ratio upon constant stirring at room temperature. Under vigorous stirring, the solution's pH was rapidly increased to pH 10 upon adding 10 ml of 25% aqueous ammonia. 10 min after the solution turned black, 10 ml of 1.0 M sodium citrate was added to the dispersion and the mixture was kept in constant reaction parameters (pH, temperature, agitation) during 30 min. For the preparation of core-shell particles, magnetite particles were used as seeds and gold was deposited onto them by citrate reduction method [21]. 1 ml of the above suspension was transferred into 100 ml of 1 mM sodium citrate solution. The solution was heated until boiling under constant stirring. When boiling, 10 ml of 0.01 M $HAuCl_4$ solution was rapidly added and the solution was stirred for 30 min while boiling. The mixture turned deep red indicating the presence of metallic gold. The colloidal suspension was cooled to room temperature and washed twice with water using centrifugation. The suspension was centrifuged at 10,000 rpm for 10 min and the supernatant containing very small size particles, excess surfactant and reaction by-products such as salts were decanted away. Bottom agglomerated particles were re-dispersed in water and the same process was repeated one more time.

Immobilization of Esterase onto the Core-Shell Nanoparticles

Lyophilized esterase suspended in water was dialyzed against 10 mM sodium phosphate buffer at pH 8. Final enzyme concentration was 8 μM. After the purification of nanoparticles, these particles were dispersed in phosphate buffer pH 8. The nanoparticles were added to the enzyme solution in a 1:10 ratio. This solution (8 μM of esterase with 0.8 μM of Fe_3O_4@Au nanoparticles in phosphate buffer pH 8, being 0.8 μM the concentration of gold present in the form of nanoparticles) was incubated overnight at 4 °C with constant mild agitation. In order to remove uncoupled esterase from the solution, the particles were separated from the solution using an external magnetic field. The recovered supernatant solution was checked for the presence of enzyme and particles using UV–visible spectroscopy. The bottom agglomerated particles were re-dispersed in phosphate buffer pH 8 and the same purification process was carried out. After the second wash, the particles were re-dispersed. The concentration of the protein was calculated from Lambert-Beer law. The enzyme's molar extinction coefficient at 280 nm is 44,600 M^{-1} cm^{-1} (http://www.expasy.org/cgi-bin/protparam1?Q3IL66@noft@). Detection of enzymatic activity was carried out using UV–visible spectroscopy. The assay mixture (0.75 ml final volume) contained 1 mM p-nitro phenyl acetate (pNPAc) in 20 mM phosphate buffer pH 8. The release of p-nitrophenol in the presence of the enzyme was continuously monitored by measuring the solution's absorbance at 405 nm for 5 min. One enzyme unit was defined as the amount of enzyme releasing 1 μmol of p-nitrophenol per minute under the described conditions. The same assay was performed with a blank sample, which contains no derivative particles and free enzyme alone in phosphate buffer pH 8.

Dynamic Light Scattering

DynaPro (Protein solution) Titan with temperature controlled MicroSampler was used for dynamic light scattering

experiments. 100 μL sample solution was pre-filtered through 0.22 μm pore size filter. The average hydrodynamic size and size distribution of the core-shell nanoparticles, enzyme and enzyme tagged nanoparticles were estimated.

Scanning Electron Microscopy

Carl Zeiss 1540XB scanning electron microscopy (SEM) with Noran energy dispersive X-ray spectroscopy (EDS) system was used for particle's size estimation and composition. SEM images were collected upon optimizing the voltage between 5 and 12 kV on silicon substrate where the dried magnetic core-shell particles were placed. The average size of the core-shell nanoparticles was estimated. X-rays, which are also produced by the interaction of electrons with the sample, were detected by EDS. The electron beam was focused over the particle projection area during the X-ray acquisition for particle's composition analysis. The X-ray spectrum was acquired for 60 s, at an acceleration voltage of 12 kV. NORAN system six version 2.0 software from Thermo Fischer scientific was used to analyze the EDS data. In the SEM data, 1 pixel corresponds to 0.56 nm.

SEM Image Analyses

For nanoparticles' SEM image analysis, an in house image processing package called BNIP-Pro was written in MATLAB version 7.3. The SEM image was baseline corrected using manually placed multiple control points in the base of the image. The image was then converted to a binary image, using a threshold value that allowed for the observation of a maximum number of separated particles. Morphological erosion and dilation was applied to the binary image in order to break residual contacts between particles. The modified binary image was then multiplied with the original image, leading to an image where only the particles are visible. Contours were drawn around all particles, and their individual area and intensity used for further analysis.

Absorbance and Fluorescence Spectroscopy

Thermo scientific UV–visible spectrophotometer (model VWK International UV1 v4.60) was used to characterize the nanoparticles, protein, protein coated nanoparticles and enzyme activity. The path length of the quartz cuvette used was 1 cm. Absorbance spectra were recorded between 220 and 800 nm. Enzyme activity was investigated by continuously monitoring light absorption at 405 nm for 5 min. The absorption values at 405 nm for free enzyme and immobilized enzyme onto the nanoparticles have been corrected upon subtraction of the absorption of the respective blank. The blank concerning the free enzyme assay included buffer and substrate in the same concentration of the free enzyme assay. The blank concerning the immobilized enzyme included buffer, substrate and nanoparticles in the same concentration of the assay of the protein-nanoparticle bioconjugate. The characterization of enzyme and enzyme tagged nanoparticles was carried out using a RTC 2000 PTI Fluorescence spectrometer at 295 nm excitation (slits set at 5 nm). The used quartz cuvette path length was 1 cm. For the characterization of the enzyme, 295 nm excitation (slits set at 5 nm width) was used in order to record the fluorescence emission spectra of the nanoparticles, enzyme and enzyme tagged nanoparticles.

Results

Characterization of Esterase Enzyme

PhEst contains a catalytic triad formed by residues Ser147, Asp225, and His258 (highlighted as grey sticks in Fig. 1) and four free cysteine residues (Cys 27, Cys 56, Cys 179 and Cys 203 displayed in black in Fig. 1). All four cysteine residues are solvent accessible, as displayed in Fig. 1. The pI of PhEst is 5.7.

Characterization of Core-Shell Nanoparticles

The stable citrate coated magnetite nanoparticles dispersion is shown in Fig. 2a (brown color dispersion, I). Figure 2a also shows the stable dispersion of gold coated magnetite nanoparticles (purple color dispersion, II, Fe_3O_4@Au core-shell nanoparticles). The magnetic nature of the gold coated magnetite nanoparticles is demonstrated in Fig. 2a (at location III) using a permanent magnet. It can be seen that the surface modified superparamagnetic nanoparticles can be easily separated from solution using an external permanent magnetic field. Moreover, the absence of the characteristic gold color in the solution after magnetic separation indicates the absence of individual gold particles. Figure 2b shows the SEM image of Fe_3O_4@Au core-shell nanoparticles. Using BNIP image analysis software package, the particles' size distribution is estimated as 22 (±5) nm (Fig. 2d). DLS measurements of freshly prepared particles diluted in phosphate buffer pH 8 revealed an average hydrodynamic diameter of 37.1 (±20) nm. The chemical composition of the particles was confirmed by EDS (Fig. 2c). Experimental analysis qualitatively confirms the presence of the elements C, O, Fe, Na, Si, Au and Cl. Na, C, and O peaks can be expected from sodium citrate surfactant; Si from the substrate; Fe, Au and O from Fe_3O_4@Au core-shell nanoparticles. The detected lines (in eV) are: C (0.281), O (0.528), Fe (0.704, 6.403), Na

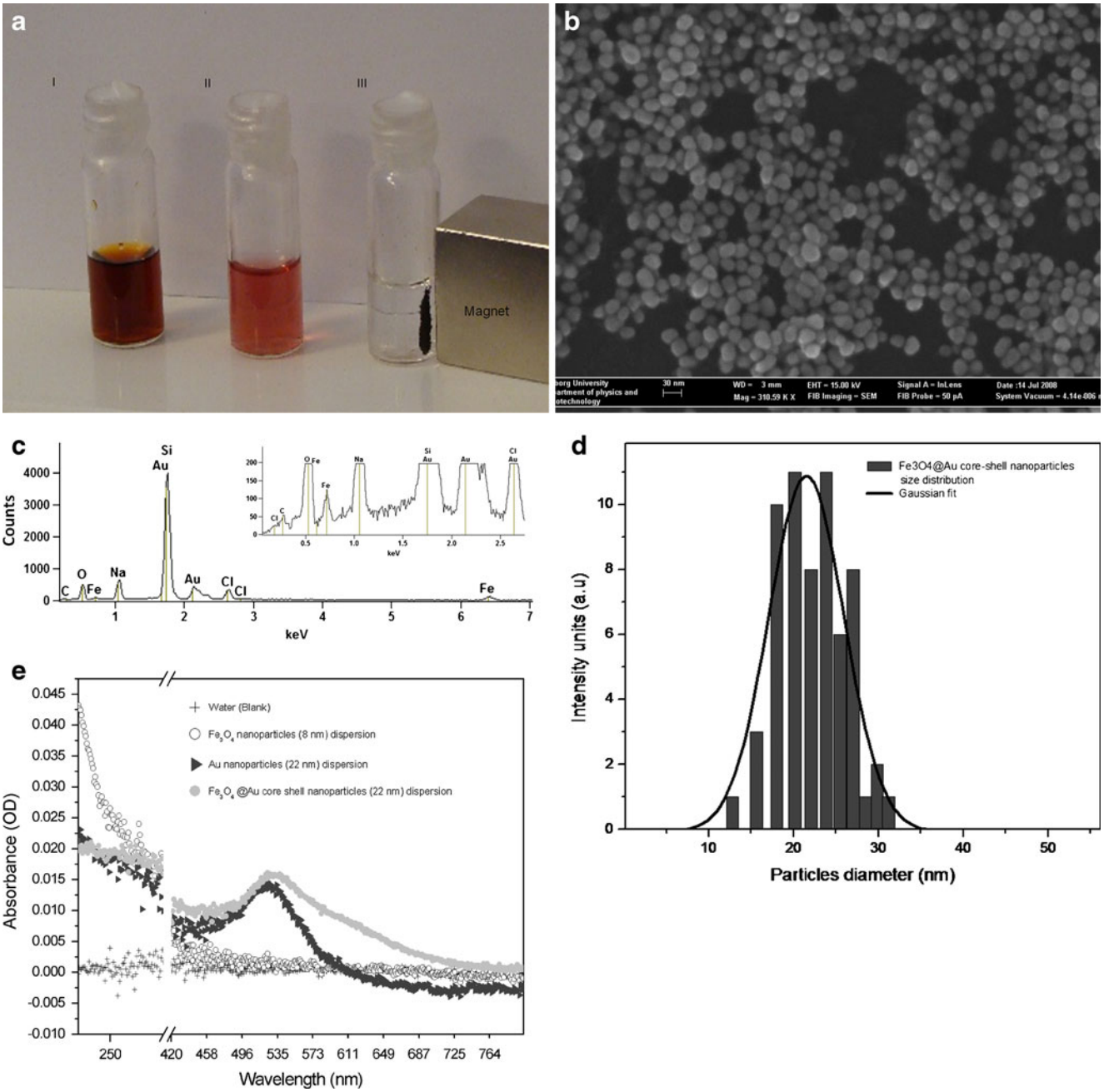

Fig. 2 **a** Display of samples containing (*I*) Magnetite dispersion (*brown*), (*II*) gold modified magnetite nanoparticles dispersion (*purple*) and (*III*) separation of superparamagnetic gold coated magnetite nanoparticles from solution using a permanent magnet, illustrating the separation potential of the technique. **b** SEM image of Fe_3O_4@Au Core-shell nanoparticles. The estimated average particle size is 22 nm. SEM images were collected upon optimizing the voltage between 5 and 12 kV on silicon substrate where the dried magnetic core-shell particles were placed. **c** EDS analysis of gold covered superparamagnetic nanoparticles. The electron beam was focused over the particle projection area during the X-ray acquisition for particle's composition analysis. The X-ray spectrum was acquired for 60 s, at an acceleration voltage of 12 kV. NORAN system six version 2.0 software from Thermo Fischer scientific was used to analyze the EDS data. **d** Particles' size distribution obtained from BNIP image analysis. **e** Absorption spectra of water (solvent blank), 8 nm average sized citrate stabilized Fe_3O_4 nanoparticles dispersion, citrate stabilized Au nanoparticles (22 nm average size) dispersion, and citrate stabilized Fe_3O_4@Au nanoparticles (average size of 22 nm) dispersion. Fe_3O_4 nanoparticles dispersion displays an absorption peak in UV region (see high absorbance at 220 nm). This peak is suppressed both in gold nanoparticles and Fe_3O_4@Au Core-shell nanoparticles Au nanoparticles dispersion absorbs maximally at 520 nm (surface plasmon resonance), while Fe_3O_4@Au core-shell nanoparticles display maximum absorbance at 534 nm

(0.041), Si (1.742), Cl (2.621, 2.81), Au (1.651, 1.665, 2.125). EDS spectrum of the silicon wafer alone showed only the presence of Si and O (data not shown). Figure 2e displays the UV–visible absorption spectra of citrate stabilized particles of Fe_3O_4 (average size of 8 nm), Au nanoparticles (average size of 22 nm) and Fe_3O_4@Au nanoparticles (average size of 22 nm) in aqueous solution and of water (blank). Fe_3O_4 nanoparticles dispersion shows an absorption band with maximum absorption at 220 nm and citrate stabilized Au nanoparticles dispersion shows typical gold absorption at 520 nm. The absorption spectrum of Fe_3O_4@Au nanoparticles shows that the characteristic gold absorption peak (surface Plasmon resonance peak) is 14 nm red shifted with maximum intensity displaced to 534 nm. This peak also displays a broad shoulder towards higher wavelengths.

Characterization of Bioconjugates Made of Enzyme (PhEst) Immobilized onto the Core-Shell Nanoparticles

DLS has been used to determine the hydrodynamic diameter (D_h) of the particles, protein and complex of protein and nanoparticles. The observed D_h were 37.1 nm (FWHM 20 nm), 49.4 nm (FWHM 30 nm) and 74.6 nm (FWHM 25 nm), respectively, confirming enzyme immobilization onto the particles (Table 1).

UV–visible spectroscopy was used in order to monitor the efficacy of the washing steps (removal of free, non-bound enzyme from the solution) and binding of the enzyme to the nanoparticles. In order to monitor enzyme binding onto the nanoparticles, absorption spectra of both the supernatant as well as of the bottom settled particles were acquired after each wash following each centrifugation. Figure 3 shows the absorption of the supernatant phase recovered after centrifugation of the first and second washing steps. The intensity of the enzyme absorbance peaks observed in the supernatant after the second wash were much smaller than the peaks observed for the bottom settled enzyme linked to the particles (Figs. 3 and 4), though the particles were diluted 500 times with buffer. Subsequent washes did not show change of the intensity of the characteristic protein peaks (220 nm, 280 nm) these

Table 1 Hydrodynamic diameter and respective FWHM obtained with dynamic light scattering for esterase alone, Fe_3O_4@Au nanoparticles alone and esterase immobilized onto Fe_3O_4@Au nanoparticles diluted in 20 mM phosphate buffer pH 8

Dynamic light scattering (DLS)	Hydrodynamic diameter (Dh) (nm)	FWHM (nm)
Fe_3O_4@Au nanoparticles alone	37.1	20
PhEst alone	49.4	30
PhEst-Fe_3O_4@Au nanoparticles	74.6	25

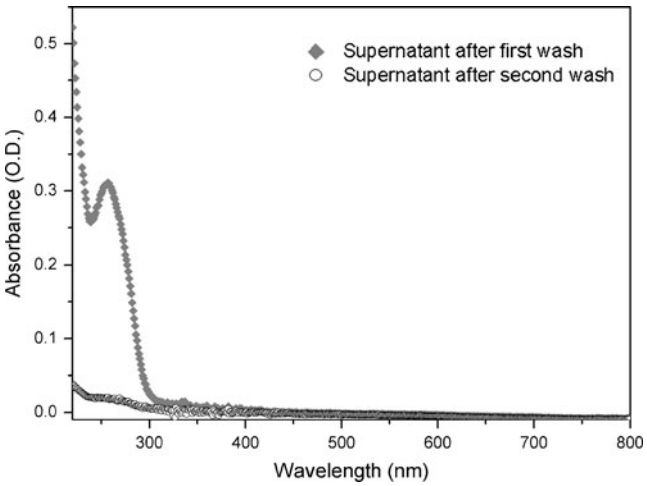

Fig. 3 UV–visible absorption of the supernatant recovered after the first and second washing steps. The spectra show the negligible amount of free enzyme present in the supernatant after the second wash

experiments suggest that two washes were sufficient to remove solubilised, non immobilized free enzyme from the solution. The larger absorption signal of esterase enzyme coupled to nanoparticles compared to the signal observed in the second wash supernatant phase confirms esterase binding to nanoparticles surface. Single distribution peak for protein-particles complex observed in the DLS data confirms the same (peak centered at 74.6 nm, FWHM 25 nm). The supernatant solutions of first and second washes do not show any peak at 534 nm region (the typical gold absorption wavelength of Fe_3O_4@Au core-shell nanoparticles) indicating the absence of Fe_3O_4@Au particles. Furthermore, data displayed in Fig. 4 also shows that the

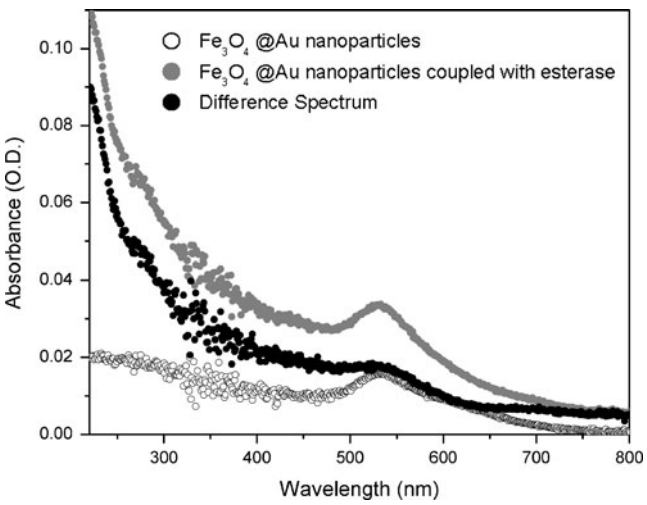

Fig. 4 Absorption spectra of Fe_3O_4@Au nanoparticles with and without esterase and the differential spectra between the protein coupled and protein uncoupled nanoparticles. The difference spectrum clearly shows the typical protein absorption peaks at 220 nm and 280 nm and the characteristic Fe_3O_4@Au absorption peak at 534 nm

protein is coupled to the nanoparticles. The absorption spectra of core-shell nanoparticles alone, esterase immobilized nanoparticles and the difference spectra have been acquired in order to confirm the presence of enzyme at the particles' surface (Fig. 4). The spectra of bare citrate stabilized core-shell nanoparticles show an absorption peak at 534 nm. The peaks in the UV range (220 nm and 280 nm) and in the visible region at 534 nm observed in the sample containing esterase coupled onto the nanoparticles are characteristic peaks of proteins and Fe_3O_4@Au nanoparticles, respectively. Normalized absorption spectra (Fe_3O_4@Au nanoparticles vs. protein derivatised Fe_3O_4@Au nanoparticles) do not show any significant change of the gold characteristic absorption peak (data not shown). The protein absorption peaks at 280 nm and in the far UV, around 220 nm, are clearly visible when the reference spectrum of Fe_3O_4@Au nanoparticles alone is subtracted (Fig. 4). These spectral features clearly confirm the presence of esterase at the nanoparticles surface. The estimated concentration of esterase immobilized onto the surface of Fe_3O_4@Au Core-shell nanoparticles was 0.986 μM. The molar ratio between nanoparticles and protein, after chemical immobilization, was 1:1.2. The colorimetric enzymatic assay confirmed the activity of the immobilised esterase. The calculated enzymatic activity was 0.12 U/ml whereas the activity of free esterase enzyme (not immobilized onto the particles) was 0.25 U/ml, showing that the immobilized enzyme is approximately 2 times more active than the free enzyme when activity is reported in U/ml.

The intrinsic protein fluorescence emission spectrum was recorded and confirmed the presence of the esterase immobilized onto the nanoparticles. The emission spectrum was obtained upon 295 nm excitation of the enzyme immobilized onto the nanoparticles and of bare nanoparticles (without enzyme molecules). The difference spectrum of the above samples is shown in Fig. 5. The spectrum has the distinct emission peak at nearly 330 nm indicating the characteristic emission wavelength of tryptophan and consequently the presence of the enzyme onto the nanoparticles surface. Figure 6 displays the normalized fluorescence emission spectra of free enzyme (not immobilized) versus the spectrum of the immobilized enzyme, showing a 5 nm blue shift of the peak of maximum fluorescence emission after protein immobilization.

Discussion

Magnetite nanoparticles were nucleated by simultaneous reaction of iron salts hydrolysis into Fe^{2+}-Ferrihydrite complex material (at pH <8) and condensation of the complex into inverse spinel structure (pH >8) leading to ferri-magnetism. During the synthesis of magnetite nanoparticles, the electron transfer between Fe^{3+} and Fe^{2+} plays a fundamental role to induce the crystallization of all the iron into spinel [22]. Moreover, particles below the critical size (~26 nm) exhibit superparamagnetic nature where the coercivity and remenence of hysteresis loop are zero. Such particles are below single domain size and in absence of external magnetic field thermal energy dominates the anisotropy energy barrier [23].

In alkaline medium, the nucleated iron oxide nanoparticles are charge stabilized with surface bound OH^- ions. The citrate anions replace the surface bound OH^- ions by ligand exchange reaction. It was suggested that the carboxylic group interacts with a trivalent iron atom located

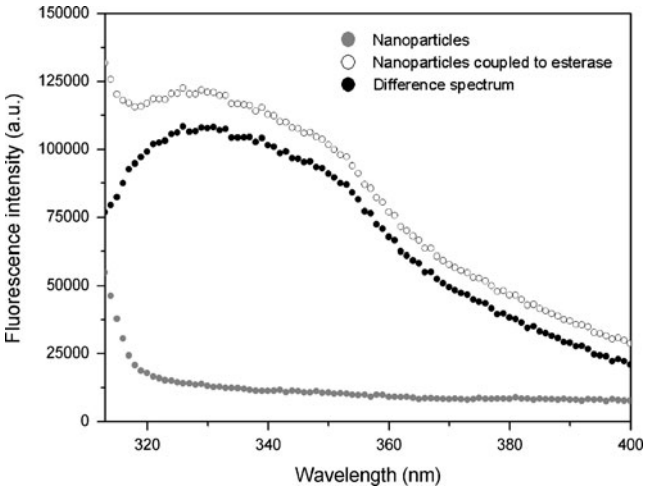

Fig. 5 Fluorescence emission spectra of Fe_3O_4@Au nanoparticles with and without esterase upon excitation at wavelength of 295 nm. Data shows the intrinsic fluorescence of the protein immobilized onto the nanoparticles

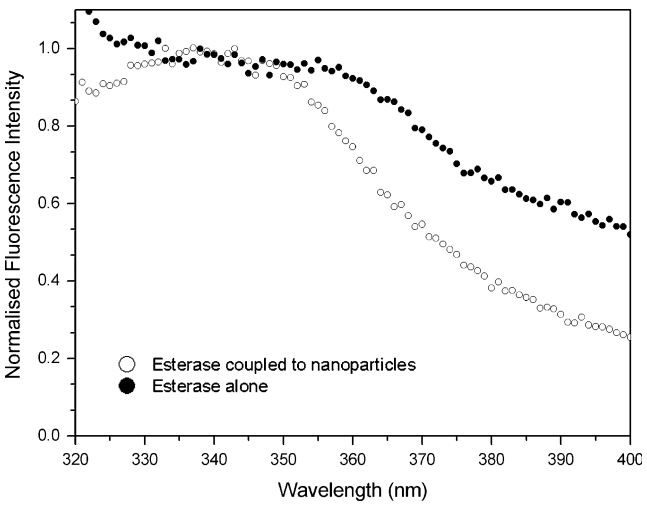

Fig. 6 Normalized fluorescence emission spectra of free esterase (not immobilized) and immobilized enzyme onto nanoparticles. The spectra show a blue shift in the fluorescence emission maximum of the immobilized enzyme

on the surface by forming a salt bridge with the two oxygen atoms [24]. Earlier work also demonstrated that citrate capped nanoparticles were stable and highly negatively charged at neutral to basic pH values, as their zeta potential value was −75 mV in pH 9 phosphate buffer solution [25]. The enzyme displays maximum activity and structural stability at pH 8. At this pH, gold covered magnetite nanoparticles (22 nm) are stable in solution. In contrast, magnetite particles (8 nm) are destabilized at pH 8 in the same buffer due to very high surface to volume ratio and magnetic dipole-dipole interactions compared to 22 nm core-shell nanoparticles. Earlier studies also confirm the coating of magnetite nanoparticle with a gold layer reduces the inter-particle magnetic dipole-dipole interactions [26]. It is also well known that free thiol groups have high affinity towards gold surfaces. Therefore, Au layer over the magnetite particles is a better choice as compared to magnetite alone for the enzyme immobilization onto superparamagnetic nanoparticles via Au-sulphur bonds.

While preparing magnetic core-shell particles, citric acid plays four major roles: 1) prevention of magnetite nanoparticles agglomeration immediately after nucleation due to affinity between carboxylic group and iron oxides, 2) reduction of the gold cations (Au^{3+}) into gold (Au^0), 3) stabilization of the Fe_3O_4@Au core-shell nanoparticles, and 4) thiol groups easily replace citrate ions on the gold surface. The gold cation in the form of $AuCl_4^-$ is a strong oxidizing agent with E^0 value of +1.002 [27]. Therefore, weaker reducing agents such as carboxylates or alcohols are sufficient to reduce these cations. Since citrate ions are weak reducing agents, the process occurs with slow reaction rate and prefers to precipitate on existing seed magnetite particles. Strong reducing agents like borohydride reduce gold salts with higher reaction rate, where the initial nucleation of the particles occur at large numbers and primary nucleation occurs instead of secondary nucleation [20, 28].

Magnetite/maghemite (oxidized form of magnetite) displays absorption band centered in the near UV and extends into the visible region due to the charge transfer transitions involving Fe^{3+}–O and Fe^{2+}–Fe^{3+} [29]. The plasmonic excitation resonance of citrate stabilized 20 nm gold nanoparticles has an absorption maximum at ~520 nm, in agreement with literature [30]. In contrast to magnetite particles, Fe_3O_4@Au particles show a clear surface plasmon band at 534 nm. Earlier works report similar red shift for gold coated magnetite nanoparticles [26, 31]. These previous studies revealed that the surface plasmon resonance property of the Au shell is dependent on its thickness. As the thickness of the gold layer increases the plasmon resonance peak gradually blue shifts towards 520 nm. Therefore, the red shift (~14 nm) of plasmon resonance peak and the suppression of magnetite absorption band in UV region for Fe_3O_4@Au nanoparticles spectrum (Fig. 2e) confirms the completely covered magnetite core with thick Au shell (more than 1 nm) [31]. EDS spectrum also confirms the particles composition as Fe, O and Au (Fig. 2c). Therefore, the magnetic nature of the wine-red colored solution clearly shows the bimetallic core-shell particles with magnetite core and gold shell. The average particle size difference between the two sets of measurements (DLS and SEM) is due to the surfactant and water layers encapsulating the particle surfaces when in solution. It is a common observation that the average diameter of the particles is less than the hydrodynamic diameter of the same particles.

The 3D structure of PhEst [18] shows that this enzyme has four solvent accessible free cysteine residues (Fig. 1). At pH 8 the enzyme thiol groups will likely be partially deprotonated (pKmodel of 9.1, and typical pKa in protein from 8 to 11) [32], thus improving their reactivity towards gold. Since thiols bind more strongly to the gold than citrate, citrates can usually be substituted by thiols. Assuming that the entropy contribution is negligible, if this assumption is valid, enthalpy values can help us to access which bond is likely to form with the gold surface. Au–S bond strength is 47 Kcal/mol compared to 30 Kcal/mol for carboxylate–Au bond [15, 32, 33]. Therefore, Au–S bond is a likely bond between the protein and the core shell nanoparticles. At this pH the esterase also shows optimal enzymatic activity [17]. Since the pI of PhEst is 5.7, at pH 8 the protein will have a negative net charge. Therefore, it is likely that the protein molecules will replace citrate molecules and interact electrostatically with the positively charge Au surface. Though there is a possibility for electrostatic interactions that consists of carboxylate-ammonium type salt bridges, salt bridges interaction energies span from 2 to 15 Kcal/mol which is weaker than Au–S bonds (47 Kcal/mol) [34]. Therefore, solvent accessible free thiol groups present in this enzyme (in Cys27, Cys56, Cys179 and Cys203 in PhEst 3ls2.pdb structure) will covalently bind to the gold nanoparticles surface. Bain et al. demonstrated that molecules carrying thiol groups can bind very efficiently onto the gold surfaces, with the thiol moiety covalently bound to the gold surface [35]. Earlier studies also demonstrated that cysteine binds onto the gold surface through the sulfur atom and the surface is thus functionalized with amino acids [14]. The reaction formally is considered as an oxidative addition of the S–H bond to the gold surface, followed by reductive elimination of the hydrogen [36].

$$R - S - H + Au_n^0 \rightarrow R - S^- Au^+ \cdot Au_n^0 + 1/2H_2$$

Murrey group [37] also demonstrated that it is easy to replace one molecule with another by using an excess of the

new molecule while providing enough heat and/or sonication. Therefore, in order to replace the citrate by esterase, the concentration of the enzyme was maintained 10 fold higher than the particle concentration in solution. Recent studies used a 250:1 ratio of BSA conjugated with another peptide and 15 nm gold nanoparticles to synthesis a large protein-nanoparticles complex [38]. However, the mentioned work proposed that not only the higher concentration of the molecules but also the long sonication or heating is required to replace the molecules [38]. Since the enzyme is very sensitive to temperature and mechanical energy, the enzyme was left in the buffer solution along with core-shell nanoparticles, overnight under slight agitation at 4 °C.

Dimer PhEst is approximately 60 kDa with a diameter around 8 nm. In literature it is reported that some of the feruloyl esterase can form tetramers [39] that will increase the D_h of the protein complex and consequently also of the enzyme-nanoparticles complex. Our data shows that the immobilized protein is in its multimeric aggregated form (average D_h 49.4 nm, see Table 1). In the case of an ellipsoid molecule or aggregate, DLS will overestimate its actual size, such that the largest dimension of the aggregate is reported as its diameter. DLS estimates average D_h values of the enzyme/gold nanoparticles complex to be 74.6 nm. This value is smaller than the sum of the average D_h of the multimeric enzyme (49.4 nm) and single particle (37.1 nm). This is expected due to the exchange of citrate and water molecules from the gold surface and due to possible protein conformational changes upon binding to the surface. The observed D_h value of particle derivatized with enzyme confirms the immobilization of enzyme onto the gold surface. Furthermore, the single distribution peak seen in DLS (centered at 74.6 nm, FWHM 25 nm, see Table 1) when analyzing the bioconjugated sample containing protein immobilized onto the nanoparticles confirms that the washing steps were efficient in removing excess, non-immobilised free protein from the sample. If there were free protein molecules in the sample after the washing steps, two distributions for protein alone and protein-particles complex would have been observed with DLS. This was not the case.

Enzymatic activity is one of the essential parameters used to confirm the effective and fruitful immobilization of the enzyme onto the nanoparticles. The observed enzymatic activity of enzyme decorated core shell nanoparticles confirmed the success of our immobilization approach. Approximately a 2 times increase in enzymatic activity (U/ml) of the immobilized protein compared to not immobilize free protein was observed. This confirms that the proteins attached themselves to the nanoparticles via the cysteine residue(s) located far from the active site, being the substrate free to access the active site. It is also possible that binding of the enzyme to the gold nanoparticles may have caused conformational changes in the protein that affect the active site conformation. The observed blue shift in the intrinsic fluorescence emission spectra of the immobilized enzyme (Fig. 6) indicates that after immobilization the protein's tryptophan residue is in an environment with lower dielectric constant such as the gold surface [40]. Furthermore, it is known that metallic nanoparticles interfere with the protein fluorescence [41], e.g. Lakovich et al. have shown that the fluorescence enhancement or quenching depends on the thickness of gold and the distance between the metallic surface and fluorophore [42]. Quenching effects have not been investigated in this study and might have led to an underestimation of coupled PhEST to the gold nanoparticle surface.

These results encourage future development of nanoparticle based protein carriers with targeted technological applications such as bioseparation, drug targeting and to improve the enzyme stability towards pH, temperature and solvents. Moreover, it was also observed that these particles coupled with protein provide higher stability against the particles permanent aggregation and it is expected because protein molecules provide steric hindrance effect along with electrostatic repulsion between particles, as polymeric surfactants.

Conclusions

We have demonstrated the immobilization of PhEst on the surface of gold coated magnetite nanoparticles using chemical immobilization technique. The immobilized esterase showed to be more active than the free enzyme (activity measured in U/ml). It is also found that the protein-nanoparticles bioconjugates are more stable in solution than non-derivatised nanoparticles since it was always possible to re-disperse them into solution after centrifugation. The non-derivatised nanoparticles aggregated as a black pellet after two centrifugation/washing steps and no longer re-disperse. Protein derivatised nanoparticles could be explored for a large number of medical, pharmaceutical and agro-food applications. Magnetic particles facilitate to control the proteins in chemical reactions like bio-catalysis, separation and drug delivery process. Super-paramagnetic iron oxide nanoparticles (used in our studies) have been approved by the Food and Drug Administration (FDA) in order to be used as MRI contrast agents. Magnetite has high saturation magnetization among the iron oxides (92 emu/g). Super-paramagnetic nature of the particles allows us to control the particles through external magnetic fields which is an essential requirement for controlled and targeted drug delivery systems. Gold shell used in our studies not only facilitates bioimaging but also allows the formation of a strong bond (45 kcal/mol) with the enzyme for more efficient biocatalysis and separation of the particles with enzyme after the process.

Acknowledgments The authors are indebted to Dr. Sabato D'Auria and Vincenzo Aurialia from Institute of Protein Biochemistry, CNR, Via Pietro Castellino, 111, 80131 Napoli, Italy for providing the enzyme.

References

1. Klabunde KJ (2001) Nanoscale materials in chemistry. Wiley, USA
2. Rao CNR, Muller A, Cheetham AK (2004) The chemistry of nanomaterial, vol 1. Wiley-VCH Verlag GmbH & Co KgaA, Weinheim
3. Park H-Y, Schadt MJ, Wang L, Lim I-IS, Njoki PN, Kim SH, Jang M-Y, Luo J, Zhong C-J (2007) Fabrication of magnetic Core@Shell Fe Oxide@Au nanoparticles for interfacial bioactivity and bio-separation. Langmuir 23:9050–9056
4. Soudarya S, Zhang Y (2008) Use of core/shell nanoparticles for biomedical applications. Rec Pat Biomed Eng 1:34–42
5. Safarik I, Safarikova M (2002) Magnetic nanoparticles and biosciences. Munatsh Chem 133:737–759
6. Baptista P, Pereira E, Eaton P, Doria G, Miranda A, Gomes I, Quaresma P, Franco R (2008) Gold nanoparticles for the development of clinical diagnosis methods. Anal Bioanal Chem 391:943–950
7. Imahori H, Fukuzumi S, Porphyrin S (2001) Porphyrin monolayer-modified gold clusters as photoactive materials. Adv Mater 13:1197–1199
8. You C-C, Agasti SS, Rotello VM (2008) Isomeric control of protein recognition with amino- and dipeptide-functionalized gold nanoparticles. Chem Eur J 14:143–150
9. Li Y, Xu X, Deng C, Yang P, Zhang X (2007) Immobilization of trypsin on superparamagnetic nanoparticles for rapid and effective proteolysis. J Proteome Res 6:3849–3855
10. Yang Z, Si S, Zhang C (2008) Magnetic single-enzyme nano-particles with activity and stability. Biochem Biophys Res Commun 367:169–175
11. Mehta RV, Upadhyay RV, Charles SW, Ramchand CN (1997) Direct binding of protein to magnetic particles. Biotechnol Tech 11:493–496
12. Koneracka M, Kopcansky P, Timko M, Ramchand CN, de Sequeira A, Trevan M (2002) Direct binding procedure of proteins and enzymes to fine magnetic particles. J Mol Catal B Enzym 18:13–18
13. Brewer SH, Glomm WR, Johnson MC, Kang MK, Franzen S (2005) Probing BSA binding to citrate-coated gold nanoparticles and surfaces. Langumuir 21:9303–9307
14. Uvdal K, Bodo P, Liedberg B (1992) L-cysteine adsorbed on gold and copper: an X-ray photoelectron spectroscopy study. J Colloid Interface Sci 149:162–173
15. Di Felice R, Selloni A (2004) Adsorption modes of cysteine on Au (111): Thiolate, amino-thiolate, disulfide. J Chem Phys 120:4906–4914
16. Aurilia V, Parracino A, D'Auria S (2008) Microbial carbohydrate esterases in cold adapted environments. Gene 410:234–240
17. Aurilia V, Parracino A, Saviano M, Rossi M, D'Auria S (2007) The psychrophilic bacterium Pseudoalteromonas halosplanktis TAC125 possesses a gene coding for a cold-adapted feruloyl esterase activity that shares homology with esterase enzymes from γ-proteobacteria and yeast. Gene 397:51–57
18. Alterio V, Aurilia V, Romanelli A, Parracino A, Saviano M, D'Auria S, De Simone G (2010) Crystal structure of an S-Formylglutathione hydrolase from *Pseudoromonas haloplanktis* TAC125. Biopolymers 93:669–677
19. Nenadis N, Zhang H-Y, Tsimidou M (2003) Structure-activity relationship of ferulic acid derivatives: effect of carbon side chain characteristic groups. J Agric Food Chem 51:1874–1879
20. Gnanaprakash G, Philip J, Jayakumar T, Raj B (2007) Effect of digestion time and alkali addition rate on physical properties of magnetite nanoparticles. J Phys Chem B 111:7978–7986
21. Lu QH, Yao KL, Xi D, Liu ZL, Luo XP, Ning Q (2006) Synthesis and characterization of composite nanoparticles comprised of gold shell and magnetic core/cores. J Magn Magn Mater 301:44–49
22. Tronc E, Belleville P, Jolivet J-P, Livage J (1992) Transformation of ferric hydroxide into spinel by iron(II) adsorption. Langmuir 8:313–319
23. Cullity BD (1972) Introduction to magnetic materials. Addison Wesley, San Francisco
24. Lesnikovich AI, Shunkevich TM, Naumenko VN, Vorobyova SA, Baykov MV (1990) Dispersity of magnetite in magnetic liquids and the interaction with a surfactant. J Magn Magn Mater 85:14–16
25. Lattuada M, Hatton TA (2007) Functionalization of monodisperse magnetic nanoparticles. Langmuir 23:2158–2168
26. Lyon JL, Fleming DA, Stone MB, Schiffer P, Williams ME (2004) Synthesis of Fe Oxide Core/Au shell nanoparticles by iterative hydroxylamine seeding. Nano Lett 4:719–723
27. Cushing BL, Kolesnichenko VL, O'Connor CJ (2004) Recent advances in the liquid-phase syntheses of inorganic nanoparticles. Chem Rev 104:3893–3946
28. Sugimoto T, Shiba F, Sekiguchi T, Itoh H (2000) Spontaneous nucleation of monodisperse silver halide particles from homogeneous gelatin solution I: silver chloride. Colloids Surf A 164:183–203
29. Schwertmann U, Cornell RM (1991) Iron oxides in the laboratory. VCH Verlagsgesellschaft, Weinheim, p 137
30. Brown KR, Walter DG, Natan MJ (2000) Seeding of colloidal Au nanoparticle solutions. 2. Improved control of particle size and shape. Chem Mater 12:306–313
31. Wang L, Luo J, Fan Q, Suzuki M, Suzuki IS, Engelhard MH, Lin Y, Kim N, Wang JQ, Zhong C-J (2005) Monodispersed core-shell Fe3O4@Au nanoparticles. J Phys Chem B 109:21593–21601
32. Creighton TE (1993) Proteins: structures & molecular properties (2nd ed). pp 293–296
33. Schmid G, Corain B (2003) Nanoparticulated gold: Syntheses, structures, electronics, and reactivities. Eur J Inorg Chem 17:3081–3098
34. Lim JK, Kim Y, Lee SY, Joo SW (2008) Spectroscopic analysis of l-histidine adsorbed on gold and silver nanoparticle surfaces investigated by surface-enhanced Raman scattering. Spectrochimica Acta Part A 69:286–289
35. Bain CD, Troughton EB, Tao YT, Evall J, Whitesides GM, Nuzzo RG (1989) Formation of monolayer films by the spontaneous assembly of organic thiols from solution onto gold. J Am Chem Soc 111:321–335
36. Ullman A (1996) Formation and structure of self-assembled monolayers. Chem Rev 96:1533–1554
37. Templeton AC, Cliffel DE, Murray RW (1999) Redox and fluorophore functionalization of water-soluble, tiopronin-protected gold clusters. J Am Chem Soc 121:7081–7089
38. Ryan JA, Overton KW, Speight ME, Oldenburg CN, Loo L, Robarge W, Franzen S, Feldheim DL (2007) Cellular uptake of gold nanoparticles passivated with BSA-SV40 large T antigen conjugates. Anal Chem 79:9150–9159
39. Benoit I, Asther M, Bourne Y, Navarro D, Canaan S, Lesage-Meessen L, Herweijer M, Coutinho PM, Asther M, Record E (2007) Gene overexpression and biochemical characterization of the biotechnologically relevant chlorogenic acid hydrolase from aspergillus niger. Appl Environ Microbiol 73:5624–5632
40. Stoller P, Jacobsen V, Sandoghdar V (2006) Measurement of the complex dielectric constant of a single gold nanoparticle. Optics Lett 31:2474–2476
41. Lakowicz JR (2006) Principles of fluorescence spectroscopy (3rd ed). Springer
42. Zhang J, Lakowicz JR (2007) Metal-enhanced fluorescence of an organic fluorophore using gold particles. Opt Express 15:2598–2606